Use of LMS Amesim® Model to Predict Behavior Impacts of Typical Failures in an Aircraft Hydraulic Brake System

Mário Maia Neto and Luiz Carlos Sandoval Góes

Department of Mechanical Engineering, Aeronautical Institute of Technology, São José dos Campos, SP, Brazil
E-mail: mario.maia.neto@gmail.com, goes@ita.br

Abstract

The brake system performs an important, safety-related function in aircraft operation throughout the world nowadays. However, the requirement of an acceptable performance and satisfactory reliability has become stricter as the aircraft landing weights and speeds increased substantially along the last decades and the regulatory authorities improved their certification basis requirements aiming a safer operation. Therefore, the brake system design, architecture and functionalities have evolved through the years and the development of the antiskid system, part of the brake system of several aircraft since 1940s, comprised an important milestone in aircraft brake system history. Besides the main function of preventing the locking of braked wheels, the antiskid system is normally also responsible for avoiding wheel braking at the instant of the first contact of the tires with ground during landing. The system also provides indication to the crew in case of system failure and helps minimize the inadvertent yaw suffered by the aircraft in case of passage of the tires on surfaces with different friction coefficients. As a result, the appropriateness of the brake system performance, which is mostly supplied by hydraulic power in recent commercial and military aircraft, shall be completely verified in normal and faulty conditions, as well as in all expected operational envelope. For that purpose, model simulations, rig tests and flight test campaigns are usually applied. Therefore, the present work aims to demonstrate the use of a computational model of a hydraulic brake system, parameterized in LMS Amesim® software, to assess the behavior of system relevant variables in normal operational conditions and the potential effects of typical failures in system performance. In addition to help support the verification process of system compliance with performance and safety requirements, such approach could also be applied for early identification of failures and operational problems still during the product development phase, highlighting the gains of applying the aforementioned tool in the context of aeronautical systems engineering.

Keywords: Brake System, Modeling, Amesim, Hydraulic, Failure.

1 Introduction

The aircraft brake system is responsible not only for decelerating the vehicle during a landing or a rejected takeoff, but it can also be applied to assist the speed control when taxiing and to park the aircraft. The use of brakes to improve ground handling due to differential braking and even to halt wheel rotation at landing gear retraction are other examples of aircraft brake system functionalities [1].

Due to their inherent advantages and installation characteristics, most of brake systems in recent commercial and military aircraft are powered by hydraulic sources. According to [2], the hydraulic system presents a high power-to-weight ratio, relatively low initial costs, acceptable maintenance levels, installation flexibility, good reliability and also the self-lubricating aspect of their components.

However, the requirement of an acceptable performance and satisfactory reliability for the brake system has become increasingly stricter as the aircraft landing weights, speeds and complexity improved substantially along the last decades. Federal Aviation Regulations CFR 14 Part 25 and MIL-HDBK-516 are examples of civil and military certification bases frequently applied during the development and certification phases of these types of airplanes throughout the world. In order to guarantee an acceptable degree of safety level on operation, certification requirements impose functional and safety-related aspects that shall be taken into consideration when developing the brake system and aircraft systems in general.

Therefore, the brake system design, architecture and functionalities have evolved through the years and the development of the antiskid system, part of the brake system of several aircraft since 1940s, comprised an important milestone in aircraft brake system history. Besides the main function of preventing the locking of braked wheels, the antiskid system is also normally responsible for avoiding

wheel braking at the instant of the first contact of the tires with ground during landing. The system also provides indication to the crew in case of system failure and helps minimize the inadvertent yaw suffered by the aircraft in case of passage of the tires on surfaces with different friction coefficients.

Basically, the antiskid control system operates by measuring the rotational speed of the aircraft wheels and actuating on the applied brake pressure. Depending on its control logic, the antiskid system is classified by [3][4] in three different categories: on-off, quasi-modulating and fully-modulating types. The on-off systems are the simplest ones and operate by releasing the brake pressure every time an incipient locked-wheel condition is detected, allowing the brake pressure reapplication only after the wheel has spun up to its synchronous speed. On the other hand, the first generation of the modulating systems, called quasi-modulating, has a control logic based on a pre-programmed sequence, in which brake pressure is held off according to skid depth, being later reapplied to a lower level and subsequently ramped up until a new skid starts. Finally, the fully-modulating systems are the most recent ones and make use of adaptive control logics. Based on the wheel-speed time history, those systems allow a better control over the optimum braking performance.

The current development of computational resources has facilitated the practice of an approach referred by [5] as "concurrent engineering", characterized by the design of products and their related processes in an integrated, concurrent manner, including their support and manufacturing. In the context of the "concurrent engineering" and motivated by the existing competitiveness in aeronautical market and the constant search for safety levels improvement, the increasing use of simulation models became practically indispensable for reducing aircraft system development cycles as well as in predicting field operational problems. Figure 1 illustrates the several applications of simulation model in product development process.

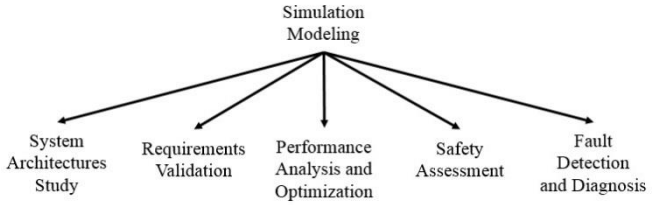

Figure 1: Simulation modeling applications

The early detection of failures in aeronautical systems has become a real necessity in order to keep its high level of safety. For that purpose, the execution of operational and functional tests of systems during maintenance tasks and the incorporation of real-time failure detection functions comprise solutions normally applied. Besides the check of system properly functioning after implementing a modification or replacing a system component, functional tests are commonly performed in aircraft systems in a periodic manner, mainly for latent failures identification. The execution of those tests is also part of predictive maintenance aiming to notice symptoms that can reveal a potential degradation of the system under investigation. On the other hand, supervisory functions, like the *built-in test* (BIT), can be incorporated in critical electronic systems to detect failure occurrences in real time. They allow corrective actions to be taken in time automatically or by the crew after the appearance of a particular alarm.

However, the nature of the failure plays a significant role in the way it is dealt. Abrupt failures are those that occur in a sudden manner and should be immediately detected in safety-related systems. Incipient failures are normally linked to component wear and take place slowly. These failures are associated with a gradual variation of a system parameter in a lower magnitude, making its detection difficult during maintenance tasks [6].

The model-based fault detection and diagnosis comprises an alternative to the aforementioned methods whose use has been growing for decades. With the advantage of eliminating the installation of physical redundancies like additional sensors coupled to the system, the model-based approach makes use of mathematical models to raise analytical redundancies for it. Its development requires, nevertheless, the compliance with some relevant requirements as the desired capability of uncoupling failures and a low sensitivity to modeling errors, which are usually considered as system unknown inputs and could lead to false alarms [6]. According to [7], wrong diagnoses resultant from imprecise or incomplete models, or even from erroneous reasoning, may also originate unnecessary maintenance actions.

Several techniques of model-based fault detection and diagnosis have been studied since 1990s. As described in [6] and [8], the quantitative methods are based on the manipulation of analytical redundancies, called "residuals", and may apply different methods like parameter estimation, parity equations and state/output observers for the determination of the real system model. An example of the construction of the "fault signature matrix", a binary matrix determined from the residuals and applied to isolate the system failures, can be found in [9]. The model-based fault detection and diagnosis techniques can also be qualitative, as illustrated in [10] by the use of knowledge-based methods and the fault signature matrix just as a starting point for the method. The temporal causal graph representation covered in [11] consists in another tool that can help in detecting and diagnosing failures in a qualitative manner. Finally, the methodology presented in [7] comprises the use of a binary matrix referred to as "D-matrix" to support the fault detection and diagnosis, which states the relationship between system failure modes and particular types of system tests, being the latter any kind of information about the system functioning state.

On the other hand, the detection and segregation of failures might not be an easy task even with the modeling support. The method's robustness to modeling errors is reduced when multiple or simultaneous failures are considered. Moreover, in order to raise mode detailed information about the failure such as its type, magnitude and cause, the contribution of a system specialist is normally required to correlate with them additional factors like equipment operational conditions, aging level, maintenance history, and so on [6][8].

Based on this background, the present work aims to demonstrate the use of a computational model of a hydraulic brake system, parameterized in LMS Amesim®, to assess the behavior of system relevant variables in normal operational conditions and the potential effects of typical failures in system performance. Due to the current availability of physical modeling software with fast simulation time, this approach could represent a good solution for a quick, preliminary assessment of system behavior on particular conditions.

The hydraulic brake system illustrated in Figure 2 comprises a system of a variable-wing fighter aircraft and will be applied for the present analysis. The technical information and test results published in [12][13] for the respective brake system will be used as reference in order to validate the nominal model developed herein.

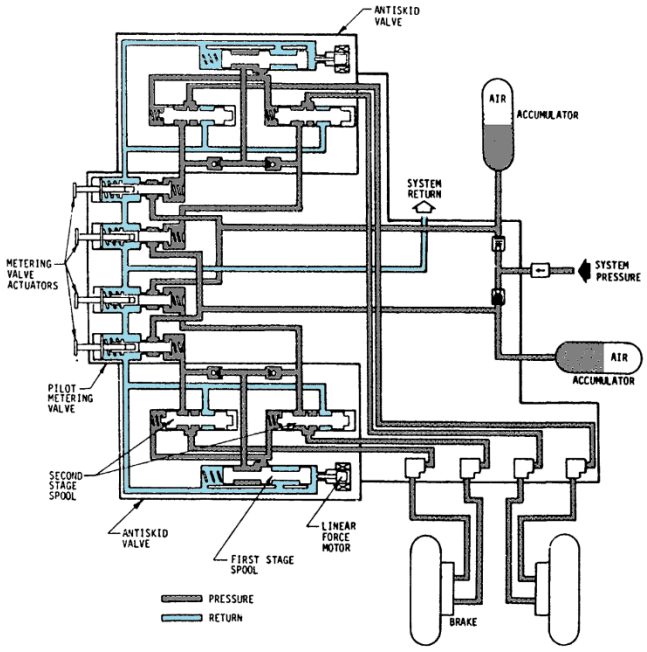

Figure 2: Hydraulic brake system schematics. Source: [13]

2 Modeling and Formulation

The brake system is supplied by the aircraft hydraulic power generation system with a 3.000-psig pressure, which is later duplicated to independently provide hydraulic power for each brake assembly. In each subsystem line, a hydraulic accumulator is installed to allow brakes application in emergency conditions or with the main hydraulic system turned off. Two antiskid valves, one for each brake assembly, and four metering valves, required by the system architecture and responsible for modulating the braking demand applied by the pilots, are located inside a unique valve assembly. The metering valve consists in a control pressure valve, whose output pressure is directly proportional to the force applied by the pilots on the brake pedals. The antiskid valve is composed of two stages and actuated in the first stage by means of a linear motor. Once the input signal is received from the antiskid system control unit, a new force balance is established in both stages of the antiskid valve, leading to the control of the hydraulic pressure resultant in the brake assemblies. Finally, each brake assembly is supplied by both hydraulic subsystems, existing a total segregation between the piston chambers operated by each subsystem in the interior of the brake assembly [13].

An equivalent hydraulic diagram of the hydraulic brake system is provided in Figure 3. For simplification purposes, the metering valves are represented by proportional directional control valves and the brake assemblies are illustrated only by a pair of hydraulic pistons. The supply and the return pressures are described as lumped sources.

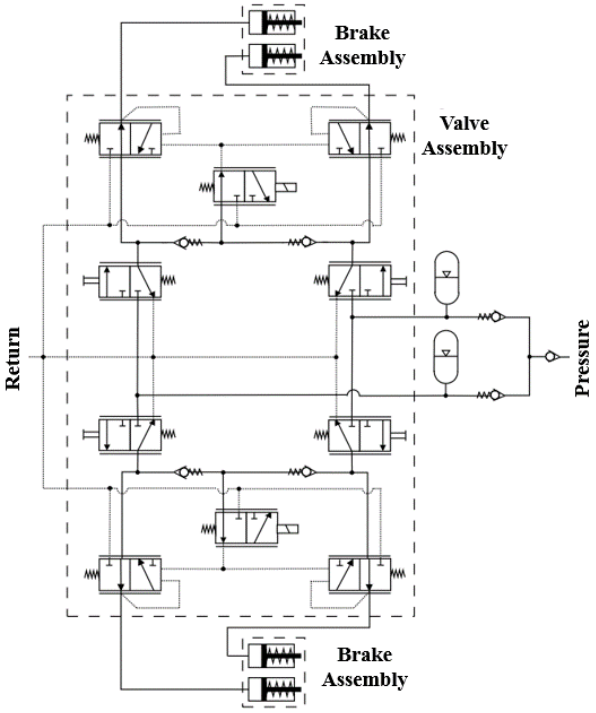

Figure 3: Brake hydraulic system diagram

The LMS Amesim® model of the diagram of Figure 3 is presented in Figure 4. The hydraulic brake system architecture shown is composed of three elements with well-defined boundaries, which are the valve assembly, the brake assemblies and the inputs blocks. Components associated with the hydraulic generation and distribution system, represented by the power source, reservoir, accumulators, tubing, hoses and a check valve, are also part of the diagram.

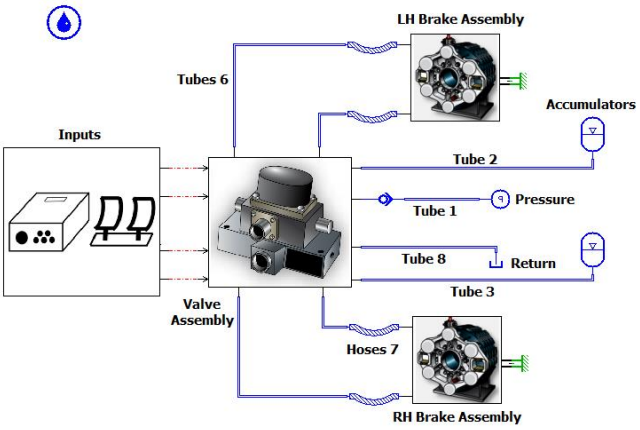

Figure 4: Brake hydraulic system model in LMS Amesim®

The basic modeling and formulation that compose the brake system model will be divided into two separated topics: the hydraulic system model and the brake assembly dynamic model. More details about the inputs block will be provided later in chapter 3, during the model validation discussion.

2.1 Hydraulic System Modeling

The components of the hydraulic generation and distribution system are described by common blocks that exist in the LMS Amesim® hydraulic library. Meanwhile a hydraulic pressure source element is applied to simulate the ideal pressure provided to the brake system by the aircraft hydraulic pump, the aircraft reservoir is modeled by means of a constant pressure source tank element. At the same time, the main hydraulic fluid properties used for flow calculations, like its viscosity, density, bulk modulus and air/gas content, are given by the indexed hydraulic fluid properties element located in Figure 4 at the top of left-hand side.

Among the main functions of the hydraulic accumulators, it is possible to highlight the supply of flow by short periods of time and the attenuation of system pressure pulsations [14]. The hydraulic accumulators of Figure 4 are modeled applying the respective element without inlet orifice, which comprises a hydropneumatics accumulator that supplies hydraulic pressure as a result of its equilibrium with the pressure of the gas located in an isolated volume within. The hydraulic accumulator element of LMS Amesim® hydraulic library considers the polytropic law of gases to calculate the gas properties inside the accumulator [15].

A hydraulic check valve with linear characteristic element is used to simulate the behavior of the check valve that exists in real system supply line. After achieving the cracking pressure, the element model makes use of a linear relationship between pressure drop and flow, without incorporating any dynamics. However, the model allows a mild hysteresis to be taken into consideration for the valve opening and closing actions [15].

The LMS Amesim® software makes available several types of models to represent the hydraulic tubes, which are basically divided into a group of models based on lumped elements and a unique option of continuous parameters modeling that solves 1D Navier-Stokes equations [15]. For the present work, a model with lumped elements is chosen to represent the hydraulic tubing, which is characterized by the segregation of flow important behavior effects like compliance, inertance and pressure drop as discrete elements, connected by means of the continuity law or specific pressure conditions.

The following equations illustrate the relationship between pressure and flow for each main effect that exist in a hydraulic line. The first effect is called *system compliance* and is related to the pressure-dependence variation that the fluid density exhibits. The ideal compliance is related to fluid flow and line pressure through eq. (1) [14].

$$C_f \triangleq \frac{\int Q dt}{P} \tag{1}$$

Due to its kinetic energy, the fluid flow exhibits another effect known as *fluid inertance*. The relation between pressure variation and fluid flow in the fluid inertance element is given by eq. (2) [14].

$$\Delta P \triangleq I_f \frac{dQ}{dt} \tag{2}$$

The last effect observed in the flow dynamics through hydraulic lines consists in the fluid resistance, also referred to as *pressure drop*. The fluid pressure drop in a horizontal straight tube and completely developed flow can be given by the semi-empirical equation of eq. (3). The first term in the right-hand side of the equation is called the "friction factor" and is dependent on tubing relative roughness and also on Reynolds number [16].

$$\Delta P = f \frac{L}{D} \frac{\rho {V_L}^2}{2} \tag{3}$$

Components like valves result in locally situated pressure drops. The relation between the fluid flow and the pressure drop through their orifices can be expressed by a non-linear equation for turbulent flows, as shown in eq. (4), or by a linear equation for laminar flows, given by eq. (5) [16].

$$Q = C_d A_o \sqrt{\frac{2}{\rho}(\Delta P)} \tag{4}$$

$$Q = \frac{2\delta^2 D_0 A_o}{\mu} \Delta P \tag{5}$$

Figure 5 describes how the hydraulic line is divided into lumped elements in LMS Amesim®, being each node characterized by the sum of each main behavior effect. For the node, the compliance, inertance and pressure drop are illustrated by their equivalent effects in a mechanical system, given by the damping, inertia and friction losses, respectively. A total of 3 (three) nodes are applied in the present model for each tube. However, the same methodology is not used for the hoses in LMS Amesim® hydraulic library. For the hose model, those effects are taken into consideration in an equivalent manner for its whole length, without segregating it into discrete nodes.

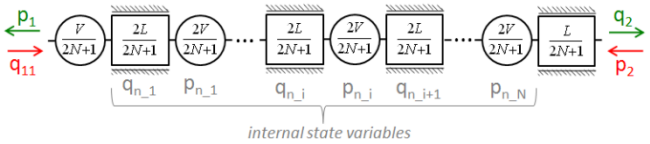

Figure 5: Internal state variables of line lumped model. Source: [15]

The LMS Amesim® software applies similar or adapted formulation from those presented herein in order to calculate the pressure and flow derivatives in the model nodes. Moreover, the software has the capability of considering the effect of flow frequency in the pressure drop calculation along the tube in a phenomenon called *frequency-dependent friction* (*FDF*). Basically, the FDF addresses the changes in laminar flow profile due to viscosity effects in high frequency flows or during quick transients, which are taken into consideration with higher or lower intensity according to the dissipation number given by eq. (6) [15].

$$D_n = \frac{\vartheta L}{cR^2} \quad (6)$$

The valve assembly internal model is shown in Figure 6. Since the metering valve actuating mechanism is not modeled in the present study, the same 2-position, 3-port hydraulic valve element of LMS Amesim® hydraulic library is applied to model the metering valves and both stages of the antiskid valves. This element comprises a 2nd order internal dynamics. With electrical operation and return by spring, the actuation signals of the metering valves and the 1st stage of the antiskid valves are supplied by the block representative of the system inputs through dimensionless connections of signal type. For simplification purposes, no feedback is assumed in the 1st stage of the antiskid valve because a 2nd order dynamics already takes place between the input signal and its spool internal position.

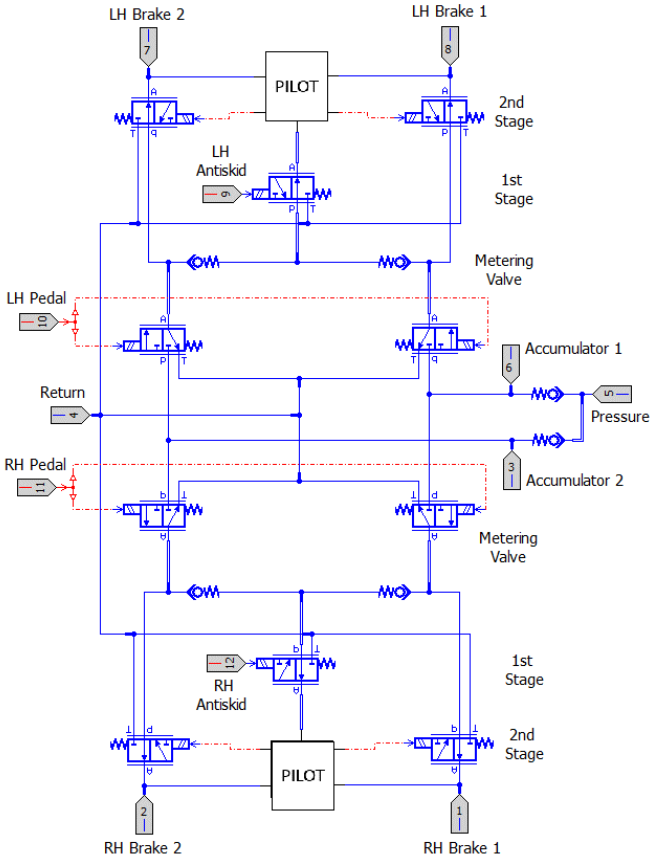

Figure 6: Valve assembly internal model

Since the hydromechanical interface between its stages is no deeply detailed in the schematics of Figure 2, a simplified model for the antiskid valve 2nd stage is adopted as illustrated in Figure 7. The modeling of an electrohydraulic servovalve with force feedback could include high order dynamics according to [16]. However, the present model considers, besides the own 2nd order dynamics of the hydraulic valve element of LMS Amesim® hydraulic library, an internal loop between the output pressures of the 1st and 2nd stages in order to define the pilot pressure of the valve 2nd stage. In Figure 7 the fixed hydraulic orifice and simple hydraulic chamber elements are used to help system stability. In practice, they might represent detailed internal characteristics of the real physical component like passage restrictions or dead volumes. Moreover, the actuation area of each pressure is weighted by means of the gain associated with each hydraulic pressure sensor element, being the resultant force simplified by a dimensionless signal responsible for operating the 2nd stage. The normalization and unit adequacy of the dimensionless control signals are done by adjusting the internal properties of the hydraulic valves blocks.

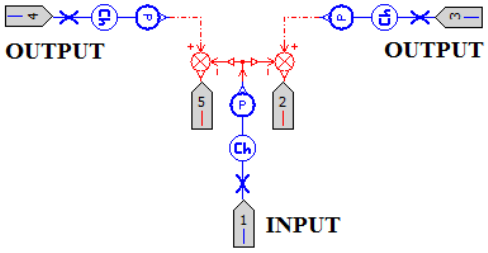

Figure 7: Pilot scheme for antiskid valve 2nd stage model

Finally, the check valves located inside the valve assembly are modeled making use of the spring-loaded check valve element of LMS Amesim® hydraulic library. The relationship between pressure drop and flow in that element obeys the pressure drop through orifices formulation but considering the change in the orifice passage area as a function of its internal spool position. The present check valve model does not incorporate any internal dynamics and, nevertheless, allows a mild hysteresis to be taken into consideration for the valve opening and closing actions [15].

2.2 Brake Assembly Modeling

In an aircraft hydraulic brake system with antiskid function, characterized by fast and cyclic braking pressure actuations, the brake assembly dynamics assumes an important role in the overall system performance. Therefore, in the current brake assembly designs, whose constructions normally apply steel or carbon disks in a multiple disk configuration, the behavior of the disk friction coefficient is extremely relevant.

The materials used in the brake assembly disk design should present particular relevant characteristics, responsible for allowing to them a satisfactory useful life, efficient heat absorption and dissipation, and an appropriate behavior in the brake torque. According to [17], properties like a consistent, high friction coefficient, low wear rate, good resistance to high temperatures, minimized volumetric expansion and high values of thermal conductivity and specific heat denote desirable characteristics for those materials.

Figure 8 describes the equilibrium of forces in a multiple-disk hydraulically operated brake assembly. With the disks totally compacted, the piston tangential brake force can be given by eq. (7). It is a function of the disk friction coefficient, the acting force resultant from hydraulic pressure application and the opposing force of the piston return mechanism. The overall brake torque can be obtained from eq. (8).

$$F_{braking_j} = 2\mu_{disk}\left(F_{action_j} - F_{return_j}\right) \quad (7)$$

$$T_{braking} = R_{piston} N_{rotors} \sum_{j=0}^{N_{pistons}} F_{braking_j} \quad (8)$$

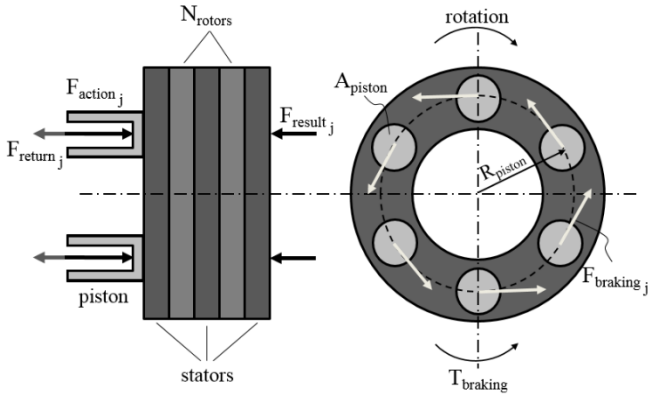

Figure 8: Forces acting on a multiple-disk hydraulically operated brake assembly

The LMS Amesim® model of brake assembly is shown in Figure 9, where a total of 6 (six) pistons is assumed for the equipment. The physical and constructive properties of each piston are represented by the mass and piston elements of mechanical and hydraulic component design libraries, respectively. The piston dynamics is also modeled by two elements of the mechanical library: an elastic contact element, responsible for simulating the piston free displacement until its contact with the disks, and by an ideal linear spring element, representing the piston return mechanism. The compacting behavior of the brake heat sink, given by the rotors and stators, is modeled in the right portion of the figure. For that purpose, mechanical elements like masses, dampers and ideal springs with variable stiffnesses are applied.

The overall internal volume of the brake assembly is split into two identical hydraulic volumes with pressure dynamics elements, being each one supplied by an independent line of the brake system and connected to a group of three pistons. Those elements are also capable of representing the volumetric variation due to pistons displacements.

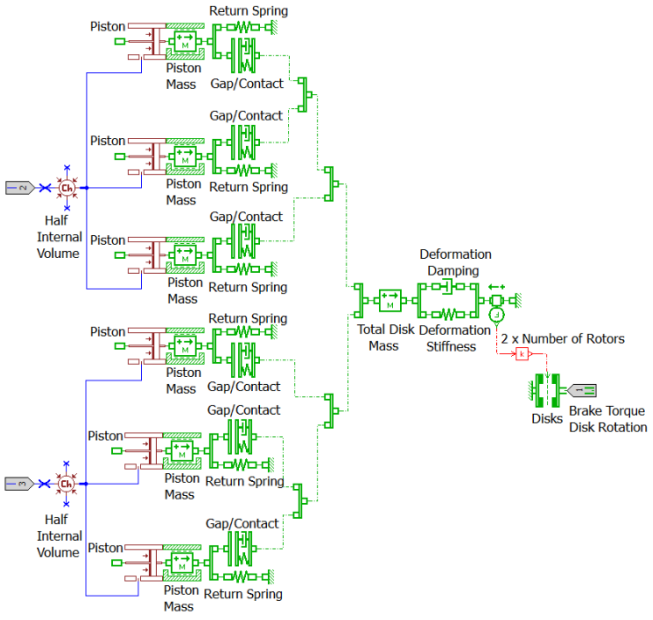

Figure 9: Brake assembly model in LMS Amesim®

Lastly, different models are available in practice to reproduce the friction behavior of the brake assembly disks. Depending on the relevant characteristics like static friction, lubricant effects and dynamic behavior, the most appropriate model can be selected and its fidelity in reproducing the brake torque real behavior shall be later validated through dedicated tests.

For the present work, the brake torque is obtained by means of the rotary Coulomb and stiction friction element from the LMS Amesim® mechanical library, which considers the wheel speed and the compacting force as inputs. Applying the reset-integrator model, it allows the stiction effect modeling through the use of a dynamic model whose integrator is introduced by means of an internal variable associated with the pre-slip displacement. The resultant brake torque given by the reset-integrator model can be represented as a function of the relative angular displacement and velocity between the contact surfaces as shown in the graphs of Figure 10. Different values for the static torque and Coulomb friction torque may be adopted in this model, as well as a continuous transition between them as known as the *Stribeck effect*. The existence of viscous friction in the static friction region may also be considered to avoid the occurrence of non-physical oscillations [15].

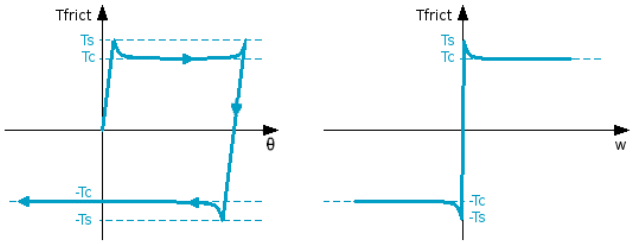

Figure 10: Friction torque as a function of relative angle and velocity. Source: [15]

3 Model Simulation and Validation

In order to guarantee the representativeness of a mathematical model, it becomes necessary to compare the simulation results with reference data, which could be taken from the literature, dedicated tests, component qualification data or even from full-scale aircraft tests.

Therefore, the information provided in [12][13] for the fighter aircraft brake system under analysis will be applied herein to validate the developed model. The studies addressed in [12][13] afford technical information and results of tests accomplished in brake systems of aircraft from 1950s and 1960s, which have become public and can be used for analysis and validation of computational models.

The simulation and validation of the hydraulic brake system model will be presented in two steps: the brake assembly and the hydraulic system behavior analyses.

3.1 Brake Assembly Analysis

The results of brake assembly nominal model validation are shown as follows. The graph of Figure 11 presents the relationship between the hydraulic volume filled inside the brake assembly and the applied brake pressure. As it can be

noticed, the simulated curve approximates satisfactorily the reference curve from [13]. Singular points like the beginning of the pressure increase when the piston return mechanism preload is surpassed by the brake pressure (at about 15 cm^3) and the stiffness increase at the effective contact between the disks (from 30 cm^3 to 40 cm^3) become the simulated curve similar to ones typically applied in brake system specifications. On the other hand, the difference noticed between them at the beginning of brake assembly pressurization could be explained by some factors like: the hydraulic dynamics resultant from the way the pressure was applied in the reference test, the definition method used for raising the tested curve, or even by some functional property change of the brake assembly used in the aforementioned test.

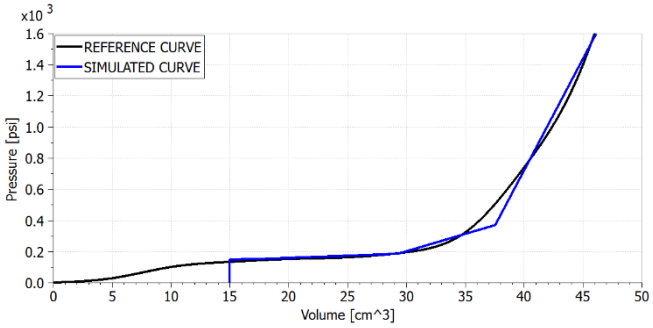

Figure 11: Brake volume x brake pressure curve

The brake torque responses for a hydraulic pressure application of 1600 psig (11.0 MPa) are shown in Figure 12 and Figure 13 for a constant rotational velocity of 1000 rpm and 1 rpm, respectively. Hydraulic pressure is applied at 0.5 second from simulation start to disregard any undesirable oscillation due to algorithm initialization.

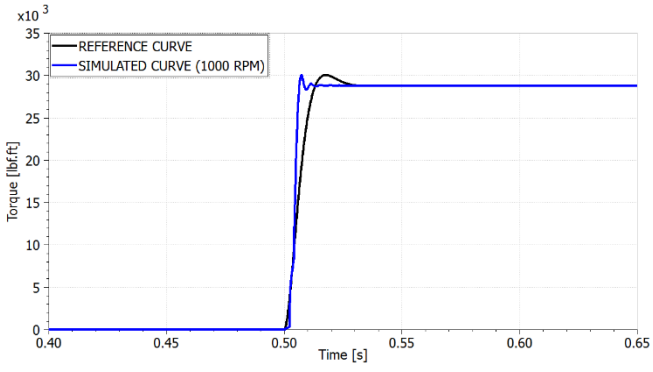

Figure 12: Brake assembly torque curve (1000 rpm)

Since the model constructed to reproduce the brake assembly performance is made out of a combination of damper and stiffness elements, the simulated output in Figure 12 does not fit exactly the 2nd order curve suggested by [12]. However, the obtained curve is considered satisfactory to reproduce the dynamic response of the brake torque because it presents the same overshoot, a few oscillations and basically the same settling time after the peak as the reference curve.

In Figure 13 a small rotational velocity is applied to the disks to allow the assessment of the static friction behavior of the brake assembly model. The validation is done by adjusting the torque peak value in that condition to be in agreement with the peak torque gain informed in [12]. On the other hand, the meaning of the peak torque gain as provided in the reference seems to be more comprehensive since [12] associates its start with a particular wheel velocity. Therefore, it could be related to a more complex behavior of the friction coefficient at low velocities during the rotors deceleration, or even to the impacts of heat sink temperature. Nonetheless, those effects are not simulated in the current model.

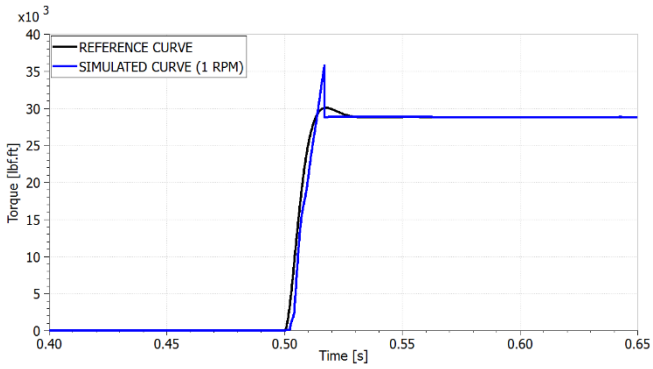

Figure 13: Brake assembly torque curve (1 rpm)

3.2 Hydraulic System Analysis

The dynamic response of the brake hydraulic system described in Figure 6 and Figure 7 is validated in three steps. Firstly, the step response of brake pressure is compared to the reference curves provided in [13], allowing the determination of most of the valve parameters in the valve assembly, mainly those related to pressure drops and dynamic responses. Afterwards, a frequency response analysis is accomplished and checked against main properties provided in [13], in order to confirm the valve assembly response is appropriate. Finally, some last adjustments are made in the antiskid valve parameters by assessing the adequacy of the provided brake pressure as a function of the valve input signal if compared to reference boundaries of [13].

The graphs shown in Figure 15 and Figure 16 describe the simulated step response in brake pressure, with a supply pressure of 1650 psig (11.4 MPa), in two different conditions: pressure increase and pressure removal. However, since it is not detailed in the reference if the pressure step was simulated by the supply pressure or by a brake pedal deflection, the latter was adopted in the present work because it better represents the system functioning principle. Figure 14 illustrates the use of piecewise linear signal source elements and constant signal elements, both from LMS Amesim® signal and control library, to simulate the metering valve and antiskid valve inputs, respectively. For the current simulation, the step input is applied in both metering valves, meanwhile the other inputs are kept null.

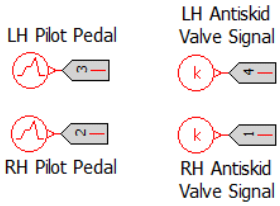

Figure 14: Input block elements for step response analysis

In both figures the pedal application or removal takes place at 0.5 second of simulation time. As it can be noticed, the simulated curve in Figure 15 approximates satisfactorily the reference curve of [13]. Dynamic characteristics like delay response time for pressure increase, rise time, overshooting and damping behavior are adequate if compared to the reference curve, which was measured in [13] during a test rig experiment. The difference between the steady state values is of only 48 psig (0.33 MPa).

An acceptable result is also obtained in Figure 16, which plots brake pressure response when the brake pedal actuation is removed. The reference curve of [13] is reproduced superimposed on the simulated graph for comparison. The only significant difference between the curves is noticed at about 0.9 second of simulation, when the model curve presents some pressure fluctuations that are not found in the reference one. Those oscillations start at the exact moment the brake assembly pistons return to their mechanical stop, which creates a phenomenon similar to suction and that could, in the real system, lead to the occurrence of a localized cavitation. The absence of that behavior in the real system curve of [13] could be explained by one or a combination of the following factors: use of a lower data acquisition rate during the test, pressure measurement in a system different point since the effect is less pronounced along the tubes that connect the assembly valve to the brakes hoses, or indeed due to a higher damping existing in the piston stop of the real brake assembly. Nevertheless, those pressure fluctuations are not relevant to the brake torque and, subsequently, to brake assembly performance because they result in a piston force that is smaller than the return mechanism preload.

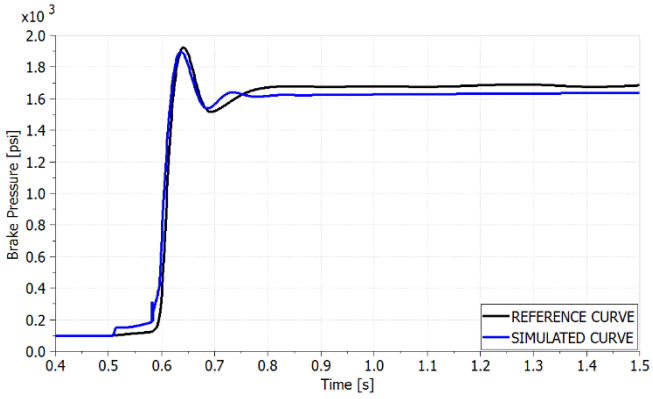

Figure 15: Step response (increase) for 1650 psig

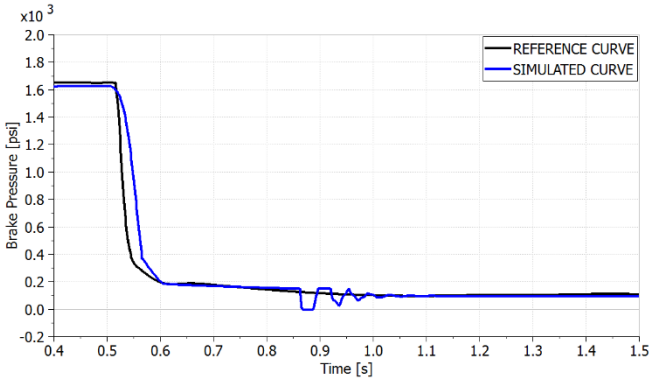

Figure 16: Step response (removal) for 1650 psig

The same brake response simulation is accomplished in other two different conditions of supply pressure, 1490 psig (10.3 MPa) and 825 psig (5.7 MPa), and compared to the main properties informed in [13] for tested curves. The obtained values and respective errors of the simulated curves are summarized in Table 1 and Table 2 for pressure increase step and removal step, respectively, for the three supply pressure conditions. The results are assessed as satisfactory.

Table 1: Step response (pressure increase)

Test Pressure (psig)	Delay Response Time (s)		Response Time to 80% of Pressure Change (s)		Percentage Overshoot of Step Change	
	Measured (1)	Error (s)	Measured	Error (s)	Measured	Error (%)
1650	0.081	0.003	0.109	-0.005	16.2	-1.1
1490	0.084	0.037	0.111	-0.009	18.8	-0.1
825	0.107	0.019	0.137	-0.006	30.4	28.8

(1) Value corresponds to the instant of pressure increase after initial step in graph

Table 2: Step response (pressure removal)

Test Pressure (psig)	Delay Response Time (s)		Response Time to 80% of Pressure Change (s)		Percentage Overshoot of Step Change	
	Measured (1)	Error (s)	Measured	Error (s)	Measured	Error (%)
1650	0.006	-0.010	0.078	0.021	0	0
1490	0.006	-0.007	0.083	0.018	0	0
825	0.006	-0.006	0.362	0.102	0	0

The next step of the validation process comprises the system frequency response, which evaluates the system steady state output when a sinusoidal input is applied. Since reference [13] does not describe in details how the oscillating pressure was supplied during the system tests, some assumptions needed to be made in the present modeling.

The oscillating input pressure is applied in the LMS Amesim® model by considering a constant value for the hydraulic pressure source element of Figure 4, equal to the maximum value within the tolerance informed by the reference, and a sinusoidal input only in the LH pilot pedal as illustrated in Figure 17. The average and amplitude values of the sinusoidal signal are adjusted in such way that, when statically simulated to its minimum and maximum values, a pressure range close to the tested one of [13] is obtained. Null values are adopted for the other inputs. The brake pressure is measured in the LH brake assembly.

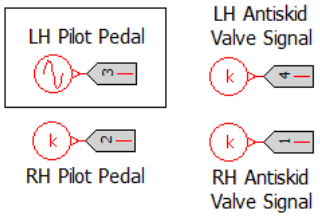

Figure 17: Frequency response analysis input elements

For the frequency response analysis, LMS Amesim® software requires the system model linearization at an operational point. Therefore, for each simulated condition, a 1-Hz input signal is applied for 5 seconds and the linearization point is defined after reaching the steady state behavior. Figure 18

shows the linearization point for the first simulated condition, which considers a 750 psig (5.2 MPa) supply pressure. For the pilot pedal input, a dimensionless signal with average of 0.73 and amplitude of 0.27 is adopted. It leads to a hydraulic pressure range of 344 psig (2.4 MPa) to 744 psig (5.1 MPa) in the brake assembly when the input is applied statically (with null frequency) at its limits. As a result, a simulation condition with an average brake pressure of about 550 psig (3.8 MPa) is obtained.

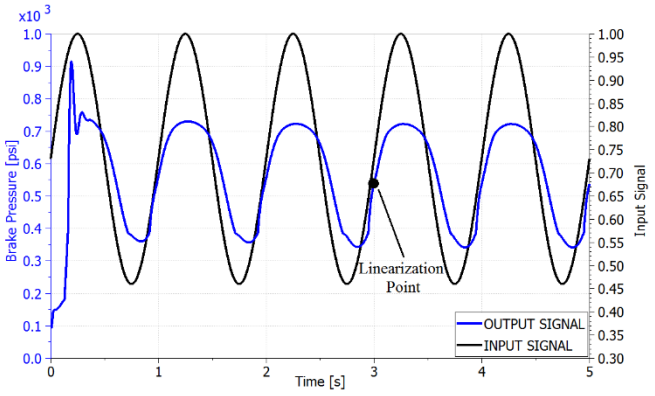

Figure 18: Linearization point for 550 psig condition

The Bode plot of the hydraulic brake system model is shown in Figure 19 for the 550 psig pressure condition. The reference frequency response, raised by test and provided in [13], is also reproduced in Figure 20.

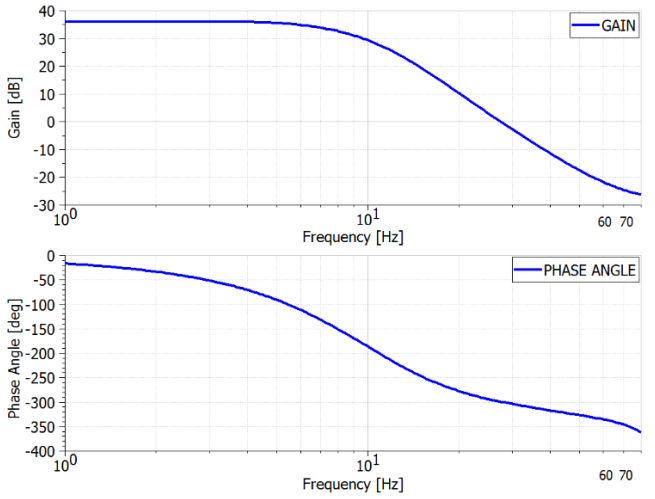

Figure 19: Frequency response for 550 psig condition

Although the gain reference curve presents a different scale, probably due to the use of another approach for applying the oscillating input pressure, it is possible to notice in Figure 19 the same very smooth resonant peak before the frequency of 8 Hz, followed by a about -40dB decay in the frequency range of 10 Hz to 40 Hz. However, the frequency response beyond 50 Hz is not modeled herein and understood as not relevant for the system dynamics. Concerning the phase angle behavior, the simulated curve in Figure 19 is considered acceptable if compared to the one illustrated in Figure 20. In general terms, both curves comprise a phase angle change from a small absolute angle, between 0º e -30º, in the frequency of 1 Hz, up to approximately -270º to -320º at 40 Hz. As a result, the gain and phase angle curves approximates reasonably the curves raised by test for practically the same test condition.

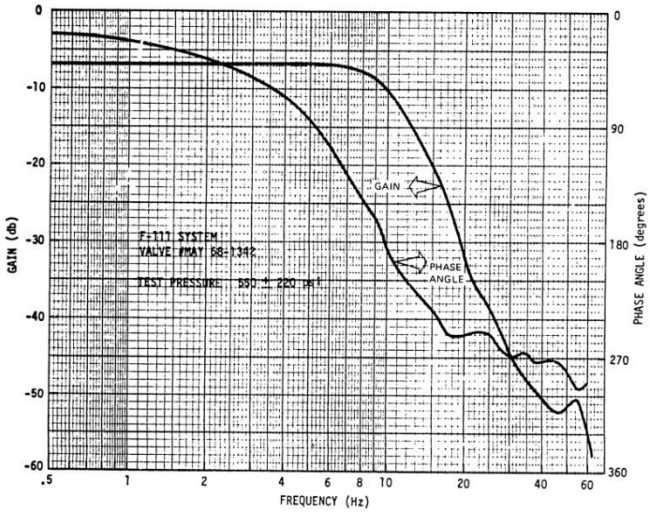

Figure 20: Reference frequency response for 550 psig condition. Source: [13]

Another test condition is also simulated considering a constant supply pressure of 1300 psig (9.0 MPa) and a dimensionless input signal for pilot brake pedal with an average value of 0.81 and an amplitude magnitude of 0.19. The resultant brake pressure ranges from 883 psig (6.1 MPa) to 1291 psig (8.9 MPa) when the input is applied statically at its minimum and maximum values. Therefore, it represents a simulation condition with an average brake pressure of about 1110 psig (7.7 MPa).

Table 3 summarizes the main properties of the frequency response determined by means of the simulational model for both operational conditions. The results comparison with the data provided in [13] is not so straightforward, because the reference presents the results of tests accomplished at four different conditions with average pressures close to the ones simulated herein but with two different amplitudes for each case. In general terms, close values for the properties are found for both simulated conditions. On the other hand, the result values shown in Table 3 have averages smaller than the ones found in the test results of [13]. Finally, it is important to highlight that, despite [13] refers to the phase angles as positive values, they are understood as negative magnitudes based on the axle orientation shown in Figure 20 and also on the own dynamics expected for the system under evaluation.

Table 3: Frequency response main properties

Reference Test Pressure (psig)	Resonant Point Frequency or -3 dB Frequency (Hz)	Gain at Resonance or -3 dB point (dB)	Phase Angle at Resonance or -3 dB (degrees)	Frequency at -90º Phase Angle (Hz)
544 ± 200	3.0	0.12	-51	5.0
1087 ± 204	3.0	0.09	-50	5.1

The last phase in the hydraulic system validation process consists in the static evaluation of the brake pressure under the antiskid valve actuation. For this purpose, the relationship between the antiskid valve input and the resultant brake

pressure is verified by applying a step input in the antiskid valve 1st stage and measuring the hydraulic pressure in the brake assembly after the necessary stabilization time has elapsed. Figure 21 illustrates the antiskid valve step input.

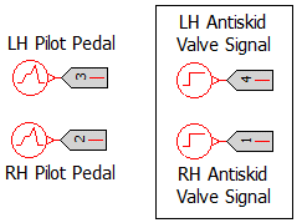

Figure 21: Input elements for antiskid valve actuation analysis

For a supply pressure condition of 1660 psig (11.4 MPa) and pilot brake pedals full application, Figure 22 depicts the brake pressure response when a step input of 46% of its total scale is introduced at 0.5 second of simulation. As it can be seen, the brake pressure presents an oscillatory transient associated with the opening kinematics of the antiskid valve, illustrated in the figure by the relative position of its 1st stage internal spool. Afterwards, due to the dynamics of the system hydraulic accumulators, the brake pressure magnitude is slowly reduced before reaching a more constant value after some seconds of simulation.

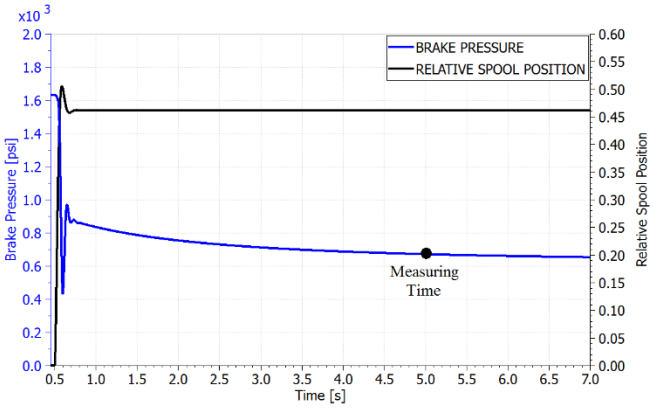

Figure 22: Brake pressure with a 46% step input in the antiskid valve

Several simulations are run with incremental improvements of 0.5 in the antiskid valve input signal and the brake pressure is measured after elapsing 5.0 seconds of simulation. Figure 22 highlights the measuring point. The same process is repeated for three distinct supply pressure conditions, that is, 1660 psig (11.4 MPa), 1020 psig (7.0 MPa) and 490 psig (3.4 MPa), and the results are plotted in Figure 23, Figure 24 and Figure 25, respectively. The expected range of system response, probably due to valve hysteresis, is provided in [13] for each simulated condition and reproduced in the figures for a better comparison. The x-axis comprises the valve input signal, which is dimensionless in the present model and has a limit value of 13.

The results obtained through LMS Amesim® computational model demonstrate a good relationship with the reference boundaries for lower and higher magnitudes of antiskid valve input signal. The main divergence is observed for intermediate input signals, when the simulated brake pressures assume values inferior to the limits informed in the reference.

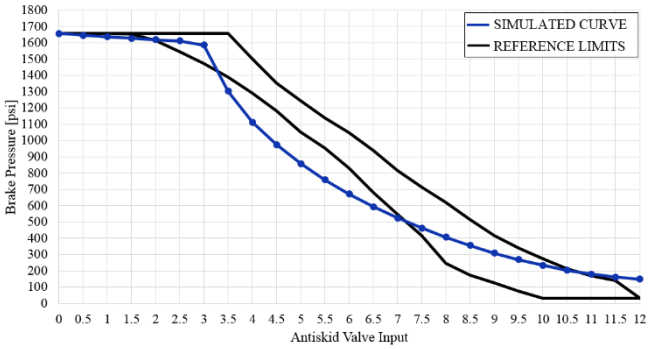

Figure 23: Brake pressure as a function of antiskid valve actuation for 1660 psig

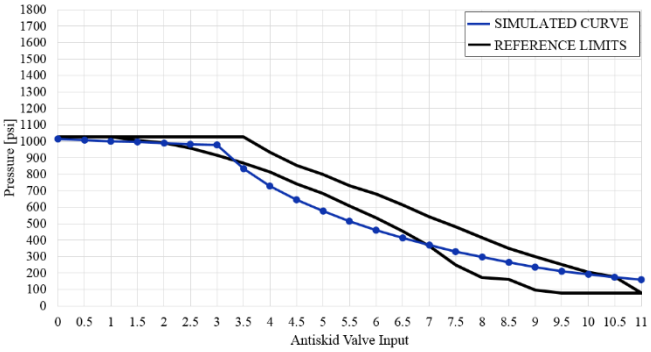

Figure 24: Brake pressure as a function of antiskid valve actuation for 1020 psig

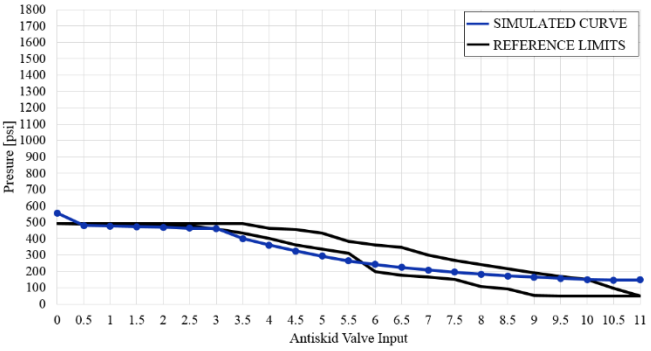

Figure 25: Brake pressure as a function of antiskid valve actuation for 490 psig

Regarding the intermediate antiskid valve input values, difference in the time adopted for pressure measurement or the own simplification adopted in the current modeling for the pilot dynamics between the antiskid valve stages are factors that might help explain the lower brake pressure values found in the simulation for those conditions. In order to illustrate the first point, simulations are repeated in Figure 26 for a supply pressure condition of 1660 psig (11.4 MPa), but reducing the measurement time to 1.0 second of simulation. As illustrated, results better adjusted to the boundaries are obtained if compared to the previous results of Figure 23.

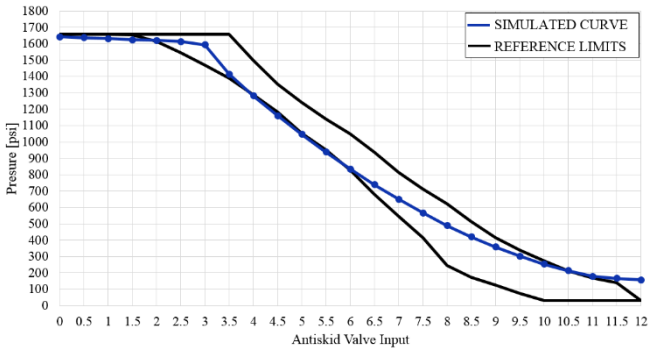

Figure 26: Brake pressure as a function of antiskid valve actuation for 1660 psig (measuring at 1.0 second)

Finally, a brake pressure higher than the supply pressure is noticed in Figure 25 for the null input condition. The justification for this behavior lies on the fact that an accumulator precharge pressure (700 psig) (4.83 MPa) higher than the supply pressure (550 psig) is adopted in the simulation. This condition, together with the presence of check valves in the system, allows the occurrence of a phenomenon similar to hydraulic lock. However, this effect does not impact the system operation since the hydraulic pressure supplied for the brake system in normal conditions (3000 psig) (20.68 MPa) is significantly higher than the one applied in that simulation case.

4 System Fault Simulation

As described in chapter 1, there are currently several structured methodologies and others ongoing studies to support the use of models in fault detection and diagnosis of aeronautical systems. Complete and well-organized processes like the ones described in [18] are also commonly applied when developing the safety assessment of aircraft airborne systems and equipment. Moreover, robust methods like the MSG-3 are nowadays used as reference for the elaboration of maintenance programs in aviation industry.

Considering this background, the present activity does not aim to replace the aforementioned methods, but just to illustrate a simplified, alternative or complementary approach to making a faster assessment of failure impacts on system behavior. The present methodology could be applied during detailed or even conceptual design phases of a system development process. It takes advantage of the current availability of physical modeling software with fast simulation times, which is exemplified herein by the LMS Amesim® model, simulated and validated in chapter 3.

This methodology is described in the flowchart of Figure 27 as divided into six steps. Each phase will be discussed as follows during the execution of an example for the brake system under analysis.

Phase 1:

Three particular failure modes are selected for the present study: a piston jam at extended position in one brake assembly, relevant internal leakage between the stages of antiskid valve, and noise in antiskid valve input signal.

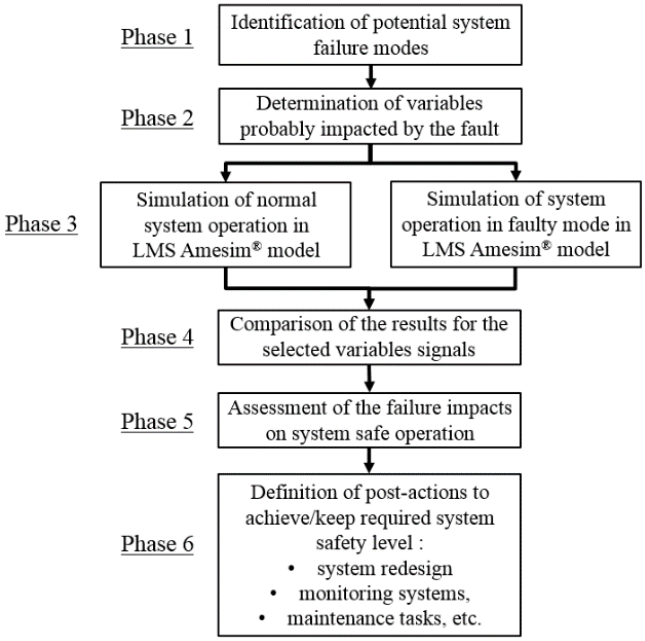

Figure 27: Simplified approach of model-based fault assessment in system operation

Phase 2:

Although more than a single variable might be impacted by each of the failure modes previously selected, only one signal per simulated failure will be chosen herein for demonstration purposes. Therefore, the brake torque will be applied to assess the impacts of the piston jam failure condition, meanwhile the brake pressure will be used to evaluate the effects of the other two failure modes.

Phase 3:

The impacts of a system failure mode shall be evaluated throughout the operational envelope. However, the current assessments will be limited to plotting only a single condition of operation for each failure mode to not be so extensive. A supply pressure of 1650 psig (11.4 MPa) is considered for the analyses.

The first simulated failure mode comprises the piston jam condition in one brake assembly. Since the gap before the beginning of disks compacting is 2.0 mm and the overall piston stroke is about 3.5 mm, it is adopted a hypothetical piston jam condition at 2.5 mm for the simulation. The implementation of this failure mode in LMS Amesim® model is straightforward, done by changing the initial displacement of one mass element of Figure 9 to 2.5 mm. In order to avoid computational errors, its lower and higher displacement limits are also updated to a small tolerance upon that value, that is, 2.4 mm and 2.6 mm, respectively. Therefore, a comparison between the brake assembly torque responses at 1000 rpm for both nominal and failed conditions is reproduced in Figure 28. The simulation consists of applying full pilot brake pedals in 0.5 second and releasing them at 1.5 seconds of simulation.

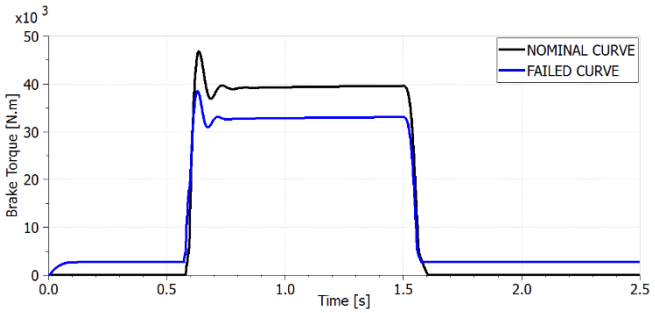

Figure 28: Brake torque response (nominal x failed)

The second failure mode to be analyzed is a significant internal leakage between the stages of one of the antiskid valves. Aiming to implement that failure, the pilot scheme shown in Figure 7 is updated for only one of the two antiskid valves by introducing a fixed laminar hydraulic orifice element between the outputs of the 1st and 2nd stages of the valve. The internal leakage implementation is depicted in Figure 29. Assuming the leakage is resultant of an increased gap in the spool bearing, the following dimensions are adopted for the orifice: 10 mm of width, 0.3 mm of clearance and 10 mm of length.

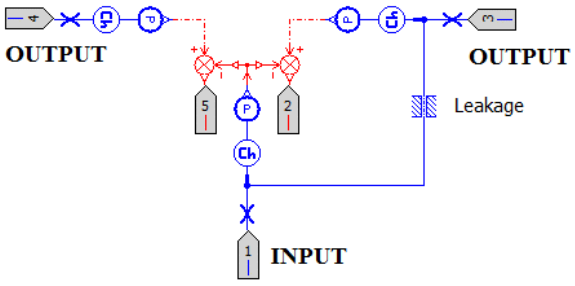

Figure 29: Antiskid valve internal leakage implementation

At first, no relevant difference is noticed in the brake pressure curves of both nominal and failed conditions when the same simulation input of the previous analysis, that is, full pilot brake pedals application in 0.5 second and release at 1.5 seconds of simulation, without any antiskid valve actuation, is applied. Therefore, a new condition is simulated considering now the actuation of the antiskid valve. For that purpose, the antiskid valve input signal illustrated in Figure 30 is used to exemplify the brake system behavior under antiskid system actuation. Full brake pedals application is assumed throughout the simulation time interval.

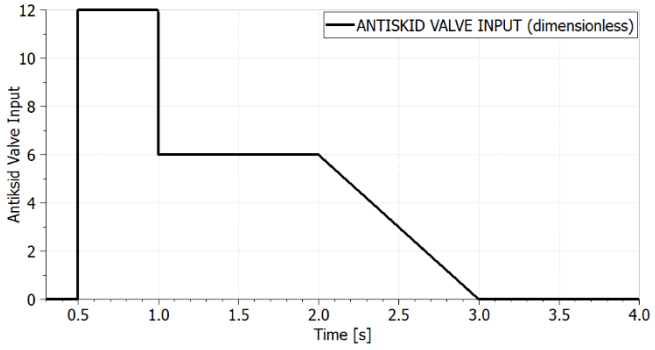

Figure 30: Antiskid valve input signal adopted for analysis

As a result, the brake pressures measured in both group of pistons of the brake assembly subjected to the actuation of the faulty antiskid valve are plotted in Figure 31. The pressure response in the other brake assembly, used herein as reference, is also provided in the same figure.

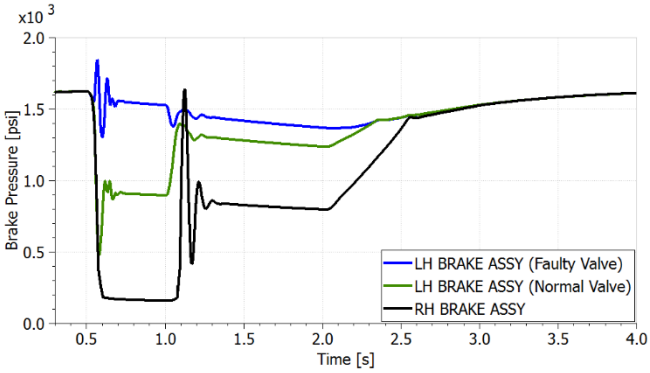

Figure 31: Brake pressure response (normal x faulty valve)

Finally, the third failure mode analysis consists in evaluating the impacts of a noisy antiskid valve input signal. That condition is simulated by adopting the same input signal profile of Figure 30, but adding a pseudo-random element in one of the antiskid valve signals as described in Figure 32. Again, full brake pedals application is considered along the whole simulation time interval.

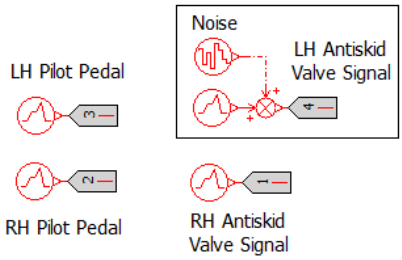

Figure 32: Noise added in LH antiskid valve signal

The resultant noisy signal of LH antiskid valve input is shown in Figure 33. A pseudo-random function of 50 Hz and amplitude equal to 1.2, which represents 10% of the maximum value of Figure 30, is adopted for the simulation.

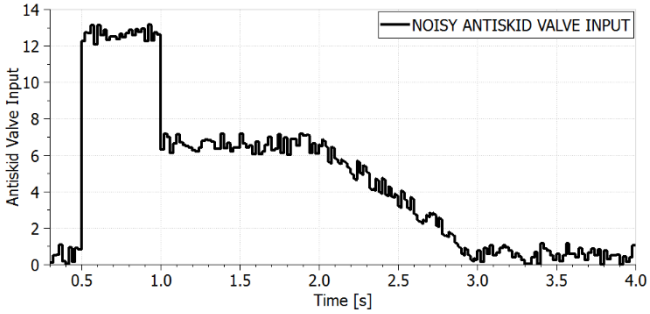

Figure 33: Noisy signal of LH antiskid valve input

The measurements of the resultant brake pressures in both brake assemblies are reproduced in Figure 34. The noisy input signal of Figure 33 is applied to the antiskid valve that operates the LH brake assembly, while the pure signal of Figure 30 is used for the RH brake assembly antiskid valve.

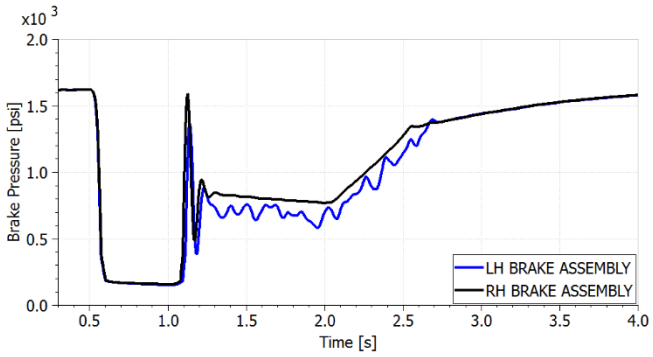

Figure 34: Brake pressure in brake assemblies (LH x RH)

Phase 4:

The two main effects of a piston jam condition in brake assembly can be noticed in Figure 28 for the brake torque behavior. For the simulated conditions, the unavailability of one piston represents a loss of 16.5% in the maximum torque value and the existence of a residual torque of 2662 N.m after brake pressure removal.

Several effects of a significant internal leakage between the stages of antiskid valve are identified through Figure 31. First of all, the leakage impacts not only the group of pistons actuated by the 2nd stage with the failure, but also the other group in the brake assembly since it is under the control of the same antiskid valve. The second effect regards the brake pressure level achieved at each stage of the antiskid system actuation. As represented by the black curve, the normal valve allows a brake pressure dump of about 90% in the first stage (from 0.6 to 1.0 second of simulation) and 50% in the second stage (from 1.5 to 2.0 seconds) if compared to the initial brake pressure at 0.3 second. On the other hand, reductions of no more than 6% in the first stage and 15% in the second stage of the initial brake pressure are achieved for the most critical group of pistons (blue curve) when the failure is present. Finally, the pressure curves of the brake assembly actuated by the faulty antiskid valve reach the final asymptotic curve in the end of cycle approximately 0.65 second earlier than the nominal curve.

The last simulated failure mode demonstrates in Figure 34 to have no relevant impact on the first stage of pressure dump (from 0.6 to 1.0 second of simulation), but the second stage is characterized by an oscillatory behavior with an average value about 14% smaller than the original curve, which lasts until simulation time reaches 2.7 seconds.

Phase 5:

The objective of the present phase is not to determine herein the severities or probabilities of the failure modes, but only to make a qualitative assessment about the potential impacts of those failures in the system safe operation.

As evaluated in the previous phase, the piston jam condition might be responsible for a reduction in the available brake torque of a brake assembly, as well as for the existence of a residual torque on it. As a result, the overall aircraft stopping distance in landing might be jeopardized by the first effect and an adverse condition referred to as dragging brake might occur due to the second effect. A dragging brake condition may eventually lead to inadvertent yaws on the ground or even to a tire burst event because of the generated heat on the tire.

Due to the abnormal behavior identified in the brake pressure curve during the operation of antiskid valve with internal leakage, the antiskid system performance is the most affected by that condition. The inability of dumping the brake pressure when required significantly impacts the antiskid system principle of operation, increasing the possibility of a wheel skid and, consequently, a tire blowout.

Lastly, the impacts of the noisy antiskid valve signal condition might not be so relevant as those of the previous failure modes. However, the present failure condition might contribute to the reduction of the antiskid system efficiency and potentially lead to some landing gear vibration issues due to the unexpected oscillations developed in the brake pressure response.

Phase 6:

A piston jam event is not a failure condition easy to be detected at real-time, except perhaps by its potential effects. The brake temperature monitoring system (BTMS) can normally identify a brake overheating due to a dragging brake during takeoff and alert the crew to not retract the landing gear on that condition, avoiding a more critical scenario for aircraft safety to take place. On the other hand, during ground maneuvers the crew will need to pay attention to any perception of inadvertent yaw in order to counteract it by means of landing gear steering and rudder pedals. Moreover, the accomplishment of regular brake assembly overhauls and the execution of system periodic functional tests may help the detection of abnormalities with the brakes pistons.

A valve internal leakage comprises a failure mode difficult to be diagnosed during maintenance tasks. Since it might have significant impacts on the antiskid system functionalities, the development of a monitoring control loop to detect the resultant effects of that failure could be a solution that needs to be evaluated and have its feasibility checked. The antiskid valve redesign aiming to minimize the impacts of an internal leakage between its stages could also be another option for further analysis.

Finally, the detection of undesirable noise in control unit signals represents one of the most challenging tasks during failure investigations. Besides the possibility of happening only at some particular operational conditions, which makes it difficult to reproduce the failure during maintenance activities, the effects of a noisy signal might not be so pronounced as those of other failure conditions. Consequently, architecture solutions to avoid noise and vibration sources, a good component qualification test campaign and the execution of several system integration tests on the aircraft might represent solutions to minimize the noise occurrence. The implementation of a health monitoring system to predict system degradation based on the measurement of the quality of relevant variables signals could also be an alternative to be studied during the system development phase.

5 Conclusions

The objective of the present work was to demonstrate the use of a computational model of an aircraft hydraulic brake system to assess the behavior of system relevant variables in normal operational conditions and the potential effects of typical failures in system performance.

The example of modeling and simulation accomplished in LMS Amesim® software seemed to be satisfactorily representative of an aircraft hydraulic brake system based on the results of the model validation process. Data from the literature for a real aircraft brake system was applied to support validation.

The current work also covered a review of aircraft brake systems, their functionalities and some methodologies currently applied for model-based fault detection and diagnoses. Moreover, a simplified approach to making a quicker assessment of failure impacts on system behavior was introduced and its main steps better described by means of some practical examples. The present methodology takes advantage of the current availability of physical modeling software with fast simulation times, which is exemplified herein by the use of a LMS Amesim® model.

Simulation of more failure mode cases and the integration of the current model with the antiskid system controller, aircraft body dynamics and wheel/tire model are instances of potential future works. In a fully-integrated model, the brake assembly and hydraulic brake system models could be deeply evaluated considering their interfaces. Besides the check of performance requirements like aircraft stopping distance, it would also allow a quantitative assessment about the failure impacts by comparing the results of efficiency parameters of the antiskid system in normal and faulty operational modes.

Finally, the topics addressed in the current work could be applied to help support the verification process of system compliance with performance and safety requirements, as well as for early identification of failures and operational problems still during the product development phase, highlighting the gains of applying them in the context of aeronautical systems engineering.

Nomenclature

A list of the variables and parameters referred to in this article is present below.

Designation	Denotation	Unit
A_o	Orifice area	[m^2]
c	Sound speed	[m/s]
C_d	Discharge coefficient	
C_f	Ideal compliance	[m^3/Pa]
D	Tube inside diameter	[m]
D_o	Restrictor orifice diameter	[m]
D_n	Dissipation number	
f	Tube friction factor	
F_{action}	Piston acting force from pressure application	[N]
F_{result}	Piston resultant force	[N]
F_{return}	Piston opposing force from return mechanism	[N]
i	Node index	
j	Index of number of pistons	
I_f	Inertance parameter	[kg.m^4]
L	Tube length	[m]
N	Number of nodes	
$N_{pistons}$	Number of pistons	
N_{rotors}	Number of rotors	
P	Line pressure	[Pa]
p_i	Pressure in node with index i	[Pa]
Q	Fluid flow	[m^3/s]
q_i	Flow in node with index i	[m^3/s]
R	Tube internal section radius	[m]
R_{piston}	Application radius of brake force	[m]
t	Time	[s]
$T_{braking}$	Brake torque	[N.m]
T_c	Coulomb friction torque	[N.m]
T_{frict}	Friction torque	[N.m]
T_s	Static torque	[N.m]
V	Tube internal volume	[m^2]
V_L	Flow velocity	[m/s]
δ	Laminar flow coefficient	
ΔP	Pressure variation	[Pa]
θ	Relative angular displacement between surfaces	[rad]
μ	Fluid dynamic viscosity	[Pa.s]
μ_{disk}	Disk friction coefficient	
ϑ	Kinematic viscosity	[m^2/s]
ρ	Fluid density	[kg/m^3]
ω	Relative angular velocity between surfaces	[rad/s]

References

[1] N S Currey. *Aircraft Landing Gear Design: Principles and Practices*, AIAA Education Series, Washington, 1998. ISBN 0930403-41-X.

[2] I Moir, and A Seabridge. *Aircraft Systems: Mechanical, electrical, and avionics subsystems integration*. 2. ed. Bury St Edmunds: Professional Engineering Publishing, 2001. pp. 91-124. ISBN 1-86058-289-3.

[3] Federal Aviation Administration. *Flight Test Guide for Certification of Transport Category Airplanes*. AC 25-7C. Washington: U.S Department of Transportation, 2012.

[4] Society of Automotive Engineers. SAE Aerospace. *AIR1739B: Information on Antiskid Systems*. Warrendale, 2012.

[5] P Khapane. *Simulation of Landing Gear Dynamics and Brake-Gear Interaction*. Thesis (Doctor of Engineering), Technischen Universität Carolo-Wilhelmina zu Braunschweig, Braunschweig. 2008.

[6] P M Frank. Fault Diagnosis in Dynamic Systems Using Analytical and Knowledge-based Redundancy – A Survey and Some New Results. *Automatica*, v. 26, n. 3, pp. 459–474, 1990.

[7] J W Sheppard, and S G W Butcher. A Formal Analysis of Fault Diagnosis with D-Matrices. *Journal of Electronic Testing: Theory and Applications*, United States, v. 23, n. 4, pp. 309-322, August. 2007.

[8] R Isermann. Model-based fault-detection and diagnosis – status and applications. *Annual Reviews in Control*, v.29, n.1, pp.71-85, 2005.

[9] K Medjaher. A bond graph model-based fault detection and isolation. In: J Andrews, C H Bérenguer, and L Jackson. *Maintenance Modelling and Applications*. Det Norske Veritas, pp. 503-512, 2011. <https://hal.archives-ouvertes.fr/hal-00635549>.

[10] J C da Silva, A Saxena, E Balaban, and K Goebel. A Knowledge-based system approach for sensor fault modeling, detection and mitigation. *Expert System with Applications: An International Journal*, v.39, n.12, pp.10977-10989, September 2012.

[11] P J Feenstra, P J Mosterman, G Biswas, P C Breedveld. Bond Graph Modeling Procedures for Fault Detection and Isolation of Complex Flow Processes. Proc. of *International Conference on Bond Graph Modelling (ICBM'01)*, SCS Publishing, v.33, pp.77-82, 2001.

[12] M K Wahi, S M Warren, and H H Straub. *An Extended Prediction Model for Airplane Braking Distance and a Specification for a Total Braking Prediction System*: Volume I. Ohio: 1977. (ASD-TR-77-6 Vol.I).

[13] M K Wahi, S M Warren, and H H Straub. *An Extended Prediction Model for Airplane Braking Distance and a Specification for a Total Braking Prediction System*: Volume II. Ohio: 1977. (ASD-TR-77-6 Vol.II).

[14] E O Doebelin, *System Dynamics: Modeling, Analysis, Simulation, Design*. Marcel Dekker, New York, 1998, pp. 54-75, 206-255. ISBN 0-8247-0126-7

[15] LMS. *AMESim Help*. AMEHelp, 2013.

[16] H E Merritt. *Hydraulic Control Systems*. John Wileys and Sons, Cincinnati, Ohio, 1967. ISBN 0-471-59617-5.

[17] D A Bailey. *Investigation of Improvements in Aircraft Braking Design*. Thesis (Doctor of Philosophy) - Cranfield University, Cranfield. 2004.

[18] Society of Automotive Engineers. SAE Aerospace. *ARP4761: Guidelines and Methods for Conducting the Safety Assessment Process on Civil Airborne Systems and Equipment*. Warrendale, 1996.